

# Chandra X-ray Observations of Galaxy Cluster A168

Yanbin Yang<sup>1</sup>, Zhiying Huo<sup>1</sup>, Xu Zhou<sup>1</sup>, Suijian Xue<sup>1</sup>, Shude Mao<sup>2</sup>, Jun Ma<sup>1</sup>, Jiansheng Chen<sup>1</sup>

yyb@bac.pku.edu.cn

## ABSTRACT

We present *Chandra* X-ray observations of galaxy cluster A168 ( $z = 0.045$ ). Two X-ray peaks with a projected distance of 676 kpc are found to be located close to two dominant galaxies, respectively. Both peaks are significantly offset from the peak of the number density distribution of galaxies. This suggests that A168 consists of two subclusters, a northern subcluster (A168N) and a southern subcluster (A168S). Further X-ray imaging analysis reveals that (1) the X-ray isophotes surrounding the two X-ray peaks are heavily distorted, (2) an elongated and continuous filament connects the two X-ray peaks. These suggest that strong interactions have occurred between the two subclusters. Spectral analysis shows that A168 has a mean temperature of  $2.53 \pm 0.09$  keV and a mean metallicity of  $0.31 \pm 0.04 Z_{\odot}$ . The metallicity is roughly a constant across the cluster but the temperature shows some systematic variations. Most X-ray, optical and radio properties of A168 are consistent with it being an off-axis merger several Gyrs after a core passage, although detailed numerical simulations are required to see whether the observed properties, in particular the significant offset between the optical and X-ray centers, can be reproduced in such a scenario.

*Subject headings:* galaxies: clusters: individual (A168) — X-rays: galaxies: clusters — X-rays: individual (A168)

## 1. INTRODUCTION

Merging of galaxy clusters is key to our understanding of the formation and evolution of not only the clusters themselves (Fabian et al. 2000; Sun et al. 2002; Fabian et al. 2003),

---

<sup>1</sup>National Astronomical Observatories, Chinese Academy of Sciences, Beijing, 100012, P. R. China

<sup>2</sup>University of Manchester, Jodrell Bank Observatory, Macclesfield, Cheshire SK11 9DL, UK

but also their member galaxies in the dense and violent cluster environment (Mihos 2004). Such merging processes can dissipate a vast amount of kinetic energy ( $10^{63} \sim 10^{64}$  erg) via different physical processes, such as heating the gas, generating intense radio and X-ray radiations (Markevitch & Vikhlinin 2001), and producing relativistic particles and magnetic fields (Vikhlinin, Markevitch, & Murray 2001; Gabici & Blasi 2003). X-ray is a unique band for studying clusters of galaxies, especially during mergers, because X-ray studies directly probe the hot intracluster medium and hence the dynamical properties of clusters of galaxies (Markevitch et al. 2002; Roettiger, Loken, & Burns 1997; Roettiger, Stone, & Burns 1999; Bekki 1999; Ricker & Sarazin 2001). X-ray is hence a powerful tool for studying the formation and evolution of galaxy clusters.

In the present paper, we report the analysis of *Chandra* observations of A168 which is located at  $01^{\text{h}}15^{\text{m}}06^{\text{s}} + 00^{\circ}19'12''$  J2000.0 (Yang et al. 2004, Paper I hereafter) with type of II–III (Bautz & Morgan 1970). Two decades ago, A168 was observed by *Einstein* IPC, and two X-ray peaks were reported (Tomita et al. 1996). Ulmer, Wirth, & Kowalski (1992) reported an unusual offset between the optical center and the X-ray center as observed by *Einstein*. They suggested that A168 was formed by the collision of two approximately equal size subclusters. Based on optical observations, In Paper I we found that the elongated shape of the X-ray emission is consistent with the spatial distribution of member galaxies. We also suggested that A168 possibly consist of two subclusters, a northern subcluster (A168N) and a southern subcluster (A168S), based on evidence from the velocity information and the luminosity function of galaxies in the cluster. In this paper, we will use *Chandra* observations to study A168. The *Chandra* data allows us to study this cluster in un-precedented details and for the first time enables us to separate clearly the emission from point sources and the diffuse hot gas. Throughout this paper, we assume a cosmology with a matter density parameter  $\Omega_0 = 0.3$ , a cosmological constant  $\Omega_{\Lambda,0} = 0.7$ , and a Hubble constant  $H_0 = 75 \text{ km s}^{-1} \text{ Mpc}^{-1}$ . In this cosmology, the cluster has a luminosity distance 186 Mpc and one arcsecond corresponds to  $\sim 0.81$  kpc. All error ranges in this paper are quoted at the 90% confidence level.

## 2. OBSERVATIONS AND DATA REDUCTION

A168 was observed twice by *Chandra* with the Advanced CCD Imaging Spectrometer (ACIS-I). The first observation, called A168\_OFFSET1 (OF1), started on 2002 January 5. OF1 was centered on  $01^{\text{h}}14^{\text{m}}52^{\text{s}}.30 + 00^{\circ}23'58''$  (J2000.0) with an exposure time of 41.12 ks. The second observation (A168\_OFFSET2, hereafter OF2), centered on  $01^{\text{h}}15^{\text{m}}25^{\text{s}}.00 + 00^{\circ}16'15''$ , was performed on November 1 in the same year with an exposure time of 38.11 ks. Both

observations were telemetered in the VFaint mode. Following the standard steps we processed the raw data with *Chandra* Interactive Analysis of Observations (CIAO, v3.0) and Calibration Database (CALDB, v2.23)<sup>1</sup>.

The data reduction for the *Chandra* observations of A168 offers some challenges. First, A168 is a faint and extended source with an angular size of at least  $12' \times 18'$ , occupying almost the whole CCD. It is hard to find a clean area to determine the background reliably. Accordingly, we have to take the blank-sky (Markevitch, Vikhlinin, & Mazzotta 2001; Markevitch et al. 2003), as the background in the spectral analysis. We also corrected for the degradation of the low energy quantum efficiency which is particularly pronounced at energies below 1 keV. Second, there is an overlap region between OF1 and OF2. It is easy to analyze the spectra in this region by extracting the spectra separately and fitting them simultaneously. However, we found from experimenting that it is not straightforward to add the images of the two observations together without creating some artifacts. We finally decided to take a simpler approach by considering only one observation in the overlap region. We then correct the exposure map for the two pointings and combine them to obtain the final image (see Figure 1). Third, because A168 is faint and extended in the X-ray, the photon noise is high at the full resolution of *Chandra*. Therefore we binned the image in  $8 \times 8$  ( $3.94''$  by  $3.94''$ ) pixels. The binned image is then cropped to a smaller area with an effective size of  $512 \times 512$  pixels.

### 3. RESULTS

#### 3.1. Imaging

Figure 2 shows the exposure map corrected and adaptively smoothed<sup>2</sup> image of A168 with point sources excluded. The 7-pixel-width gaps between CCD chips and the CCD boundaries are cut for their high unreliability. The image is smoothed by requiring the signal-to-noise ratio (SNR) to equal 6 with a Gaussian kernel; the SNR is defined as  $\text{SNR}(r) = (C - AC_{\text{bg}}) / \sqrt{(\sqrt{C})^2 + A\sigma_{\text{bg}}^2}$ , where  $C$  is the total count within an aperture  $r$  (in units of pixel), which is taken to be the scale of the smoothing kernel,  $A$  is area, i.e., the number of pixels within the aperture,  $C_{\text{bg}}$  is the mean counts of background, and  $\sigma_{\text{bg}}$  is the variation of background.  $C_{\text{bg}}$  and  $\sigma_{\text{bg}}$  are estimated from the three box regions in Figure 2. The typical smoothing scale of  $\sim 6$  pixels ( $\sim 24''$ ). In the most luminous region the scale is  $2 \sim 3$  pixels.

---

<sup>1</sup>CIAO and CALDB can be found at website of <http://cxc.harvard.edu>.

<sup>2</sup>We refer the `csmooth` algorithm to <http://cxc.harvard.edu/ciao/ahelp/csmooth.html>.

The maximum smoothing scale is taken to be 10 pixel, resulting in low SNRs ( $\sim 1$ -2) in regions where the photon counts are close to the background count rate.

Clearly, Figure 2 shows that A168 in X-ray has two X-ray peaks, peak A and peak B. These two X-ray peaks have an angular separation of  $\sim 13'.6$ , corresponding to a projected distance of 676 kpc. We also notice that the X-ray emissions around the two X-ray peaks are heavily distorted. Figure 2 also shows an elongated filamentary structure connecting these two peaks with a prominent clump in the middle. To show the significance of the filament, we study the photon counts in the dashed rectangle shown in Figure 2. We divide the  $x$ -axis into 20 bins, and count the photon events along the  $y$ -axis for each bin with the background counts subtracted. To allow for the gap between CCDs, we normalize the counts by the total number of pixels in each bin. The result is shown in Figure 2a, which suggests that emission from the filament is significant. We repeat the same procedure in the  $y$ -direction (shown in Figure 2b), the photon counts indicate that the filament extends continuously from the south to north.

For further analysis, we divide the emission into three energy bands. Figure 3 shows the contours of the soft (0.3-1.5 keV), medium (1.5-2.5 keV) and hard (2.5-10 keV) bands together with a 3-color image combined linearly from these bands. The color image shows some structures which are suggestive of slight temperature variations across A168; we address this question in the next subsection. It is worth noting that there is a small blue clump located to the northeast of peak B (see Figure 3c and the contours of the hard band).

### 3.2. Spectrum and Temperature Map

The X-ray emission from the hot gas in clusters of galaxies is thought to be from thermal bremsstrahlung, which is usually described by a MEKAL model (Kaastra & Mewe 1993; Liedahl, Osterheld, & Goldstein 1995). We therefore perform our spectral analysis using a single temperature WABS(MEKAL) model in the XSPEC package (v11.2.0). The absorption column density is fixed to the Galactic value,  $N_{\text{H}} = 3.4 \times 10^{20} \text{ cm}^{-2}$  (Dickey & Lockman 1990), as the intrinsic absorption in the cluster is likely to be small. All the following spectra are analyzed in the 0.5-0.8 keV energy range with the point sources removed. The corresponding background spectra of source spectra are extracted separately from the corresponding blank-sky regions on the CCD.

We first investigate the global temperature and metallicity of A168. We define an overall region by the boundary of the thin-solid boxes in Figure 1. From the spectral fitting, the mean temperature and metallicity are found to be  $2.53 \pm 0.09 \text{ keV}$  and  $0.31 \pm 0.04 Z_{\odot}$ ,

respectively. The mean temperature is in agreement with previous work by David et al. (1993) which gives  $kT = 2.6^{+1.1}_{-0.6}$  keV. The total luminosity is  $(0.39 \pm 0.01) \times 10^{44}$  ergs/s over the 0.01-80 keV energy range. The temperature and luminosity are consistent with the modest mass of cluster (see Table 3). White, Jones, & Forman (1997) gave a total luminosity of  $(1.13 \pm 0.03) \times 10^{44}$  ergs/s in the same energy band but for a cosmology with  $H_0 = 50 \text{ km s}^{-1} \text{ Mpc}^{-1}$ ,  $q_0 = 0.5$  and a metallicity of  $0.4Z_\odot$  (by assumption). If we convert our results to their cosmology, we find that  $L_x \sim 0.78 \times 10^{44}$  ergs/s for the diffuse emission and  $L_x \sim 0.23 \times 10^{44}$  ergs/s for the point sources; the total luminosity is  $1.01 \times 10^{44}$  ergs/s, in good agreement with their value. Notice that the point sources contribute about 23% of the total luminosity. Without the resolutions of *Chandra*, these point sources will be difficult to separate from the diffuse X-ray emission.

We next define a main body of A168 and divide it into 7 regions that are marked as region A-G from south to north in Figure 1 (thick-dashed boxes). The spectra of the regions are extracted separately. The photon count in each region is about 4000-5000 cts on average. Region C and D has about twice the counts because the spectra are extracted from both observations (OF1 and OF2). The fitting results are listed in Table 1 and plotted in Figure 4. As can be seen, the metallicity is consistent with a constant from south to north. while the fitted temperature appears to vary from south to north with region C having the highest temperature. To further investigate the temperature variation, we increase the region under study and divide it into 35 smaller boxes as shown in Figure 1 (thin-solid boxes). The average count in each box is about 1300 (in the overlap region, the counts may be twice as large), which are too few to constrain both the temperature and metallicity reliably. As the metallicity is consistent with a constant according to the above analysis, we fix it to the mean value,  $0.31 Z_\odot$  (see the above text or Table 1), and concentrate on the temperature variation. The fitting results are listed in Table 2. A temperature map (shown in Figure 5) is obtained through interpolation using the Kriging method<sup>3</sup>. We performed various  $\chi^2$  tests to check the significance of the temperature variations. It appears that region G has a significant lower temperature than other regions (A-E, see Fig. 4) while other temperature variations have less statistical significance.

## 4. DISCUSSION

In Sect.1 we mentioned that A168 is thought to be formed by the collision of two subclusters. This was first suggested from the unusually large offset between its X-ray and

---

<sup>3</sup>A function in the Winsurf 7.0 software (Oliver & Webster 1990).

optical centers (Ulmer, Wirth, & Kowalski 1992). In paper I we found evidence for the existence of two subclusters (A168N and A168S) in the optical from the luminosity function and velocity distribution of galaxies in the cluster. As we argue below, *Chandra* X-ray observations further strengthen the conclusion.

In Figure 6, we show a comparison of the optical and X-ray emissions. Peak A is associated with the cD galaxy UGC 797, the brightest member. Peak B is very close to an elliptical galaxy GIN 061, the second brightest member galaxy. Table 3 collects the relevant properties of these two peaks and their associated galaxies and subclusters. In the SLOAN *r*-band, the two associated galaxies have a luminosity ratio of 2.5 : 1. However, in the radio, UGC 797 is roughly a factor of ten fainter than GIN 061 at 1.4 GHz (Condon et al. 1998). The absolute magnitude of GIN 061 and its radio properties suggest that it may be a dominant galaxy of its local region.

D/cD galaxies are commonly found in the evolved clusters or groups (Morgan, Kayser, & White 1975; Albert, White, & Morgan 1977), and they usually coincide with the X-ray peak in the center of regular relaxed clusters of galaxies (Morgan & Lesh 1965; Bautz & Morgan 1970; Jones et al. 1979; Beers & Geller 1983; Oegerle & Hill 2001). However, in A168, while both dominant galaxies are clearly associated with X-ray peaks, both show significantly offset from the surface number density peak of the galaxy distribution. This is illustrated in Figure 7, where we superpose the X-ray emission on the contours of the distribution of member galaxies (cf. Paper I). The number density peak of galaxies is located almost in the middle of the two X-ray peaks. The offset between the optical and X-ray centers clearly indicates that A168 is not a relaxed cluster. Notice that the projected distance between the two dominant galaxies is 676 kpc, comparable to the scale of clusters. The large separation implies that these two galaxies must have formed separately in different clusters and hence have distinct evolution histories.

The luminosities of the two X-ray peaks are comparable (see Table 3), with a luminosity ratio of  $L_x^A/L_x^B \approx 1.5$ . Between the two X-ray peaks, *Chandra* observations reveals an elongated and continuous filament connecting the two, suggesting that strong interactions have occurred between the two clumps. The existence of the two peaks (A and B) in both the X-ray and radio, and the X-ray filament connecting the two peaks strongly suggest that A168 consists of two interacting subclusters, A168N and A168S.

Table 3 collects some dynamical properties of A168N and A168S. The mean velocity difference is only  $264 \pm 142 \text{ km s}^{-1}$ , which is small compared with the observed radial velocity dispersions ( $\sigma_r \sim 600 \text{ km s}^{-1}$ ), suggesting that the main bulk motion between these two subclusters is perpendicular to the line of sight. In Paper I we showed that the two components are gravitationally bound at the 92% confidence level under a linear two-body

model (Beers, Geller, & Huchra 1982). This result further supports the interaction between the two subclusters.

From contours of image (Figure 6), one can see that the innermost regions of the two X-ray peaks are roughly symmetric, but the outer contours surrounding two X-ray peaks are distorted, but the distortions are not exactly along the line connecting the two X-ray peaks. As the cluster temperature is not very high ( $kT \sim 2.53$  keV), the potentials of the two subclusters are not very deep, so their outer contours may be easily distorted in the tidal interaction. Furthermore, the filament and the prominent clump along it (see Fig. 5) can be interpreted as the tidal-stripped gas from two subclusters. These structures may also reflect the distribution of unrelaxed dark matter, similar to the ridge discovered in A1367 (Sun & Murray 2002). Ricker (1998) and Ricker & Sarazin (2001) have studied off-axis mergings of two comparable clusters. Comparing with their results (cf. their Figs. 4-9), the X-ray emission morphology of A168 resembles that of an off-axis merger with a mass ratio from 1 : 1 to 1 : 3 several Gyrs after a core passage.

We do not detect other significant changes of gas dynamics, such as shocks, strong temperature variations, as expected during merging (Roettiger, Loken, & Burns 1997; Ricker & Sarazin 2001). Moreover, we do not find any radio lobes or haloes (see Marvel, Shukla, & Rhee 1999, Figure 2c) which are considered to be related to the merging or cooling activities of clusters of galaxies (Fabian et al. 2000; Fujita et al. 2002). Furthermore, if the merger is ongoing, enhanced and concentrated blue galaxies are expected to be observed (Dressler & Gunn 1988), but Tomita et al. (1996) concluded that there are no significant blue galaxies related to the merger. The lack of activities seem to be consistent with the view that the last major collision (core passage) has occurred several Gyrs ago and the merging signatures have ‘decayed’. However, it is not clear whether this timescale is correct. We can estimate the timescale to be  $\sim 0.6$  Gyr if we take the distance of two X-ray peaks to be 676 kpc, and assume a colliding velocity of  $\sim \sigma_r \sim 600$  km s $^{-1}$ . Such a short time scale would be difficult to reconcile with the lack of strong merging signatures as some simulations show that the remnant signatures may last several Gyrs (Roettiger, Loken, & Burns 1997; Ricker & Sarazin 2001). The most puzzling feature of A168 remains the fact that the density peak of the galaxy number distribution seems to be in the middle of the X-ray peak, this appears to be rare in numerical simulations where the X-ray peaks and the dark matter density peaks (and presumably the galaxy distribution) usually coincide (Ricker 1998; Ricker & Sarazin 2001).

## 5. SUMMARY

We have analyzed the data from *Chandra* observations of A168. The mean temperature and metallicity are  $2.53 \pm 0.09$  keV and  $0.31 \pm 0.04 Z_{\odot}$ , respectively. The total luminosity of A168 is  $(0.39 \pm 0.01) \times 10^{44}$  ergs/s over the 0.01-80 keV energy range. We divided the system into many regions and studied their images and spectral properties. Our main findings are as follows:

1. Two X-ray peaks with a projected distance of 676 kpc are resolved unambiguously. The luminosity within an aperture of  $49''$  and over 0.5-8.0 keV energy range is  $(0.62 \pm 0.05) \times 10^{42}$  ergs/s for peak A and  $(0.41 \pm 0.04) \times 10^{42}$  ergs/s for peak B.
2. A significant and continuous filament with a prominent clump in the middle is detected between the two X-ray peaks.
3. No significant metallicity gradient is seen across the cluster. There is some variation in the temperature with region C having the highest temperature and region G having a significantly lower temperature than other regions (cf. Fig. 4 and 5).

The radio, optical and X-ray data for A168 strongly suggest the existence of two subclusters, A168N and A168S. The X-ray morphology is consistent with it being an off-axis merger of two comparable subclusters several Gyrs after a core passage. But it is not clear whether the lack of other merging signatures in the X-ray (such as strong shocks) is consistent with this scenario. A168 may be a very unusual system as the significant offset between the X-ray and optical centers is rare. It will be a challenge to see whether numerical simulations can reproduce the observed X-ray properties, down to a spatial resolution of  $\sim 0.4$  kpc at the full resolution of *Chandra*. More future observations of *Chandra* or *XMM-Newton* and detailed numerical simulations will shed further insights on the nature of the system.

We would like to thank the referee for valuable suggestions. We thank Drs. Xiangping Wu, A.C. Fabian and Bo Qin for their valuable suggestions. We are also grateful to Drs. Haiguang Xu, Jiasheng Huang, Xiaofeng Wang, Zhengyu Wu, and especially Mr. Albrecht Rüdiger, for helpful discussions. This research has made use of the *Chandra* X-ray databases and the NASA/IPAC Extragalactic Database (NED). This work is supported by the National Key Base Sciences Research Foundation under the contract TG1999075402 and is also supported by the Chinese National Science Foundation (NSF) under the contract No. 10273007.



## REFERENCES

- Albert, C. E., White, R. A., & Morgan, W. W. 1977, *ApJ*, 211, 309
- Bautz, L. P. & Morgan, W. W. 1970, *ApJ*, 162, L149
- Beers, T. C., Geller, M. J., & Huchra, J. P. 1982, *ApJ*, 257, 23
- Beers, T. C. & Geller, M. J. 1983, *ApJ*, 274, 491
- Bekki, K. 1999, *ApJ*, 510, L15
- Condon, J. J., Cotton, W. D., Greisen, E. W., Yin, Q. F., Perley, R. A., Taylor, G. B., & Broderick, J. J. 1998, *AJ*, 115, 1693
- David, L. P., Slyz, A., Jones, C., Forman, W., Vrtillek, S. D., & Arnaud, K. A. 1993, *ApJ*, 412, 479
- Dickey, J. M. & Lockman, F. J. 1990, *ARA&A*, 28, 215
- Dressler, A. & Gunn, J. E. 1988, *IAU Symp. 130: Large Scale Structures of the Universe*, 130, 311
- Fabian, A. C. et al. 2000, *MNRAS*, 318, L65
- Fabian, A. C., Sanders, J. S., Allen, S. W., Crawford, C. S., Iwasawa, K., Johnstone, R. M., Schmidt, R. W., & Taylor, G. B. 2003, *MNRAS*, 344, L43
- Fan, X., et al. 1996, *AJ*, 112, 628
- Fujita, Y., Sarazin, C. L., Kempner, J. C., Rudnick, L., Slee, O. B., Roy, A. L., Andernach, H., & Ehle, M. 2002, *ApJ*, 575, 764
- Gabici, S. & Blasi, P. 2003, *ApJ*, 583, 695
- Jones, C., Mandel, E., Schwarz, J., Forman, W., Murray, S. S., & Harnden, F. R. 1979, *ApJ*, 234, L21
- Kaastra, J. S. & Mewe, R. 1993, *A&AS*, 97, 443
- Liedahl, D. A., Osterheld, A. L., & Goldstein, W. H. 1995, *ApJ*, 438, L115
- Markevitch, M., Vikhlinin, A., & Mazzotta, P. 2001, *ApJ*, 562, L153
- Markevitch, M. & Vikhlinin, A. 2001, *ApJ*, 563, 95

- Markevitch, M., Gonzalez, A. H., David, L., Vikhlinin, A., Murray, S., Forman, W., Jones, C., & Tucker, W. 2002, *ApJ*, 567, L27
- Markevitch, M., et al. 2003, *ApJ*, 583, 70
- Marvel, K. B., Shukla, H., & Rhee, G. 1999, *ApJS*, 120, 147
- Mihos, J. C. 2004, in *Carnegie Observatories Astrophysics Series, Vol. 3: Clusters of Galaxies: Probes of Cosmological Structure and Galaxy Evolution*, ed. J. S. Mulchaey, A. Dressler, & A. Oemler (Cambridge: Cambridge Univ. Press), p. 278 (astro-ph/0305512)
- Morgan, W. W. & Lesh, J. R. 1965, *ApJ*, 142, 1364
- Morgan, W. W., Kayser, S., & White, R. A. 1975, *ApJ*, 199, 545
- Oegerle, W. R. & Hill, J. M. 2001, *AJ*, 122, 2858
- Oliver, M. A., & Webster, R. 1990, *INT. J. Geographical Information Systems*, 4, 313
- Ricker, P. M. 1998, *ApJ*, 496, 670
- Ricker, P. M. & Sarazin, C. L. 2001, *ApJ*, 561, 621
- Roettiger, K., Loken, C., & Burns, J. O. 1997, *ApJS*, 109, 307
- Roettiger, K., Stone, J. M., & Burns, J. O. 1999, *ApJ*, 518, 594
- Sun, M., Murray, S. S., Markevitch, M., & Vikhlinin, A. 2002, *ApJ*, 565, 867
- Sun, M. & Murray, S. S. 2002, *ApJ*, 576, 708
- Tomita, A., Nakamura, F. E., Takata, T., Nakanishi, K., Takeuchi, T., Ohta, K., & Yamada, T. 1996, *AJ*, 111, 42
- Ulmer, M. P., Wirth, G. D., & Kowalski, M. P. 1992, *ApJ*, 397, 430
- Vikhlinin, A., Markevitch, M., & Murray, S. S. 2001, *ApJ*, 551, 160
- White, D. A., Jones, C., & Forman, W. 1997, *MNRAS*, 292, 419
- Yang, Y., Zhou, X., Yuan, Q., Jiang, Z., Ma, J., Wu, H., & Chen, J. 2004, *ApJ*, 600, 141
- Zhou, X., et al. 2003, *A&A*, 397, 361

Table 1: Temperatures and metallicities for the 7 regions (defined in Fig. 1) and the whole region.

| Region       | Temperature (keV)      | Metallicity ( $Z_{\odot}$ ) | $\chi^2/\text{d.o.f.}$ |
|--------------|------------------------|-----------------------------|------------------------|
| A            | $2.48^{+0.29}_{-0.27}$ | $0.24^{+0.14}_{-0.11}$      | 168/122                |
| B            | $2.80^{+0.32}_{-0.30}$ | $0.28^{+0.17}_{-0.13}$      | 182/158                |
| C            | $3.09^{+0.23}_{-0.21}$ | $0.39^{+0.11}_{-0.09}$      | 381/333                |
| D            | $2.90^{+0.19}_{-0.16}$ | $0.24^{+0.08}_{-0.07}$      | 406/341                |
| E            | $2.74^{+0.14}_{-0.15}$ | $0.35^{+0.09}_{-0.07}$      | 349/281                |
| F            | $2.59^{+0.21}_{-0.21}$ | $0.43^{+0.15}_{-0.12}$      | 220/174                |
| G            | $1.75^{+0.10}_{-0.10}$ | $0.42^{+0.13}_{-0.10}$      | 210/142                |
| whole region | $2.53^{+0.09}_{-0.09}$ | $0.31^{+0.04}_{-0.04}$      | 1569/1006              |

Table 2: Temperatures (in units of keV) for the 35 boxes as indicated in Figure 1; the metallicity has been fixed to  $0.31Z_{\odot}$  in the spectral fitting.

|    | C1                     | C2                     | C3                     | C4                     | C5                     |
|----|------------------------|------------------------|------------------------|------------------------|------------------------|
| R1 | $3.15^{+4.53}_{-1.49}$ | $3.56^{+2.75}_{-1.21}$ | $1.60^{+0.10}_{-0.10}$ | $1.61^{+0.18}_{-0.18}$ | $2.37^{+1.97}_{-0.82}$ |
| R2 | $2.32^{+0.99}_{-0.43}$ | $2.15^{+0.46}_{-0.34}$ | $2.74^{+0.33}_{-0.27}$ | $2.20^{+0.32}_{-0.22}$ | $1.75^{+0.24}_{-0.18}$ |
| R3 | $2.42^{+0.35}_{-0.22}$ | $2.50^{+0.24}_{-0.21}$ | $2.75^{+0.20}_{-0.20}$ | $2.67^{+0.25}_{-0.26}$ | $2.72^{+0.54}_{-0.44}$ |
| R4 | $2.77^{+0.42}_{-0.39}$ | $3.12^{+0.44}_{-0.38}$ | $2.73^{+0.24}_{-0.24}$ | $2.93^{+0.29}_{-0.25}$ | $2.98^{+0.48}_{-0.35}$ |
| R5 | $2.66^{+0.47}_{-0.39}$ | $3.52^{+0.54}_{-0.47}$ | $2.77^{+0.26}_{-0.25}$ | $2.85^{+0.46}_{-0.29}$ | $3.37^{+0.71}_{-0.53}$ |
| R6 | $2.92^{+1.16}_{-0.74}$ | $2.97^{+0.71}_{-0.45}$ | $2.21^{+0.35}_{-0.24}$ | $2.98^{+0.68}_{-0.43}$ | $1.82^{+0.31}_{-0.20}$ |
| R7 | $4.08^{+3.81}_{-1.39}$ | $4.13^{+2.69}_{-1.29}$ | $2.46^{+0.37}_{-0.30}$ | $2.45^{+0.48}_{-0.31}$ | $2.36^{+1.67}_{-0.67}$ |

Table 3: Statistics of A168N and A168S.

|  | Peak A  | Peak B  | References |
|--|---|---|------------|
| (Ra., Dec.) J2000.0                    | 01 <sup>h</sup> 14 <sup>m</sup> 57 <sup>s</sup> .81 + 00°25′45″ | 01 <sup>h</sup> 15 <sup>m</sup> 15 <sup>s</sup> .92 + 00°12′54″ |            |
| Projected distance from A to B         | $676h_{0.75}^{-1}$ kpc  |   |            |
| $L_x$ ( $10^{42}$ ergs/s) <sup>a</sup> | $0.62 \pm 0.05$   | $0.41 \pm 0.04$   |            |
| Associated galaxy                      | UGC 797   | GIN 061   | (1)        |
| $m_r$                                  | 13.58   | 14.59   | (2)        |
| $M_r$                                  | −22.77  | −21.76  |            |
| Radio flux at 1.4 GHz (mJy)            | $4.5 \pm 0.6$   | $43.0 \pm 1.4$  | (3)        |
| Diameter (arcmin)                      | $0.9 \times 0.9$  | $0.58 \times 0.5$   | (1)        |
| $v_r$ (km s <sup>−1</sup> )            | $13460 \pm 26$  | $13553 \pm 30$  | (1)        |
| Associated subcluster                  | A168N   | A168S   | (4)        |
| $v_r$ (km s <sup>−1</sup> )            | $13065 \pm 113$   | $13329 \pm 86$  | (4)        |
| $\Delta v_r$ (km s <sup>−1</sup> )     | $264 \pm 142$   |   | (4)        |
| $\sigma_r$ (km s <sup>−1</sup> )       | $564 \pm 90$  | $613 \pm 56$  | (4)        |
| $M$ ( $10^{14} M_\odot$ )              | $2.1 \pm 0.7$   | $2.5 \pm 0.5$   | (4)        |

References: (1) NASA/IPAC Extragalactic Database (NED); (2) Sloan Digital Sky Survey (SDSS), Data Release 2 (DR2); (3) Condon et al. (1998); (4) Yang et al. (2004).

<sup>a</sup>The flux is calculated over the 0.3-8.0 keV energy range within an aperture of 49″ (~ 40 kpc), as indicated by two circles in Figure 2.

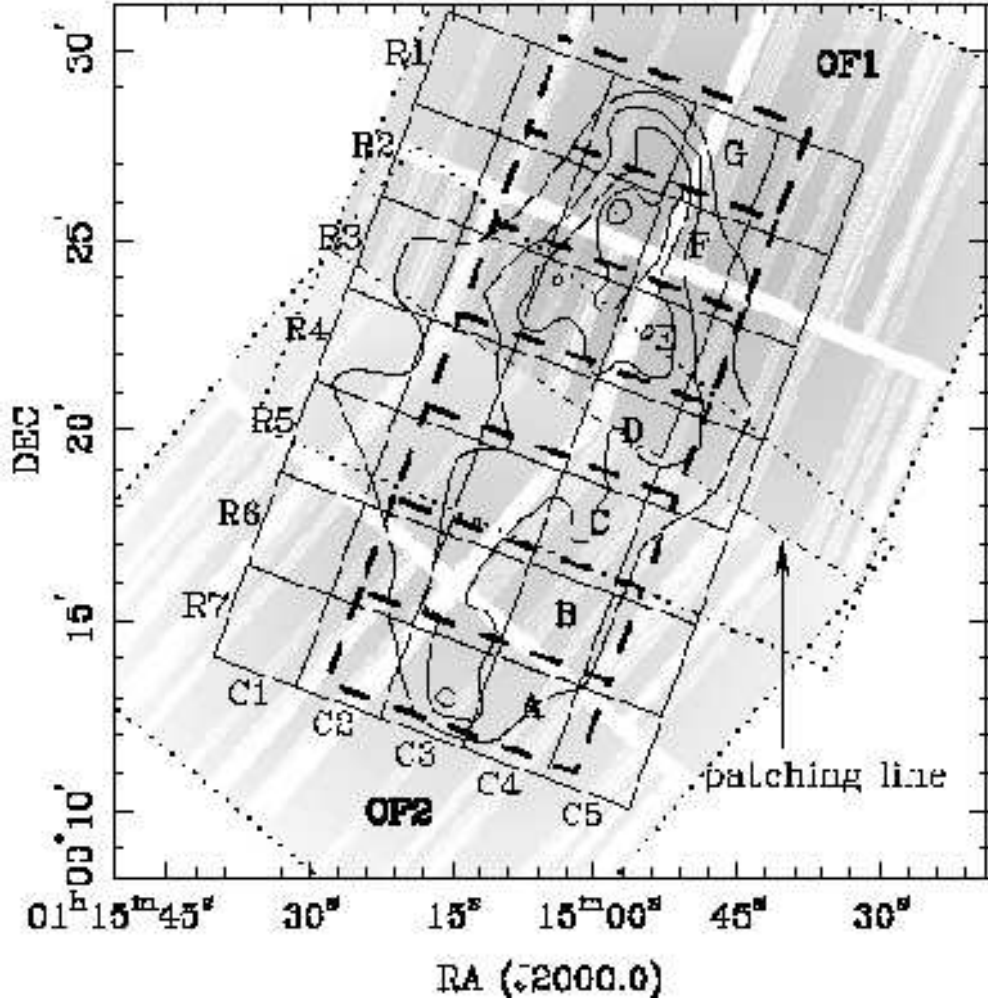


Fig. 1.— Dotted lines show the CCD field of view for each observation, OF1 and OF2. The background image is a mosaic exposure map with CCD gaps excluded. This image also demonstrates the mosaic style of the ACIS-I image of A168 along the patching line. Thin-solid lines and thick-dashed lines indicate the regions used for spectral analysis (see Sect. 3.2 and Tables 1 and 2). A rough contour of smoothed image (Figure 2) is shown for the comparison with regions of spectral analysis.

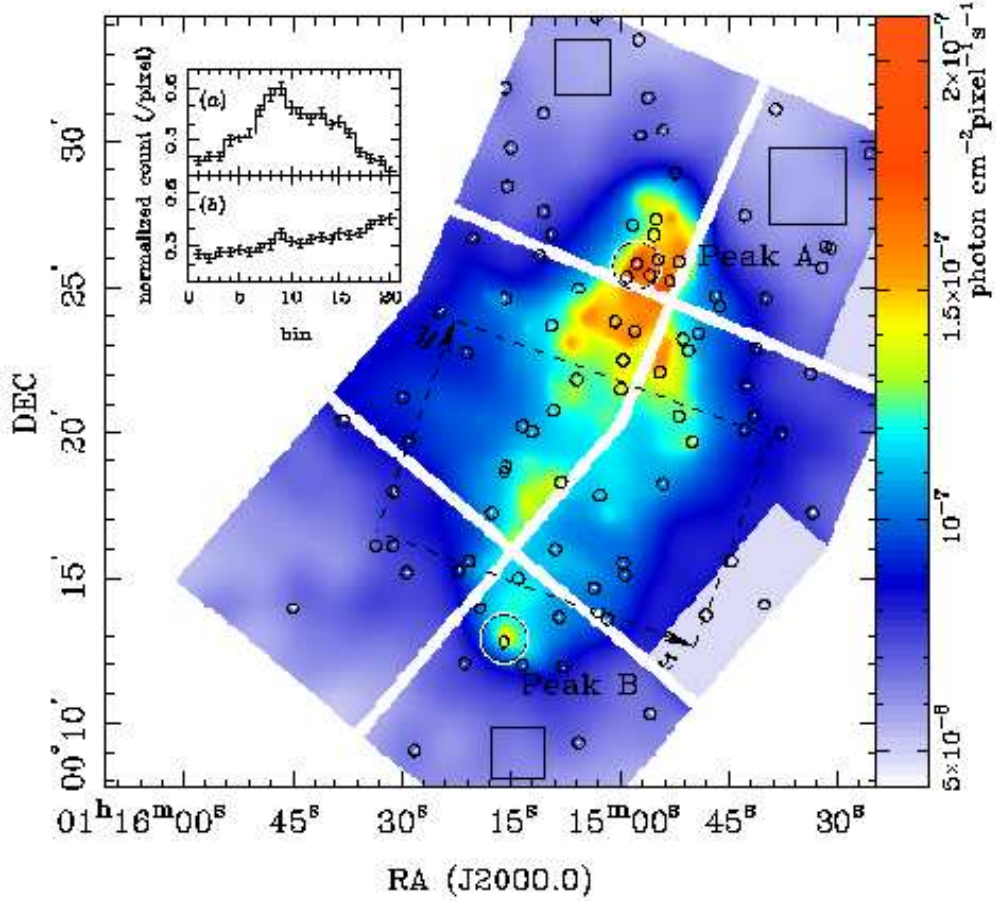


Fig. 2.— The exposure-map corrected and adaptively smoothed ACIS-I image of A168 in the 0.3-10 keV band (CCD gaps have been excluded). The three regions used for estimating the mean value and variation of background are shown in boxes. The dashed rectangle is used to check the significance of the filament (see Sect. 3.1 for details). The counts along the  $x$  and  $y$  axes of the rectangle are shown in the top left inset, (a) and (b), respectively. The two circles indicate the apertures used for measuring the flux for the two peaks. The small circles (with points at the center) indicate removed point sources. [See the electronic edition of the Journal for a color version of this figure.]

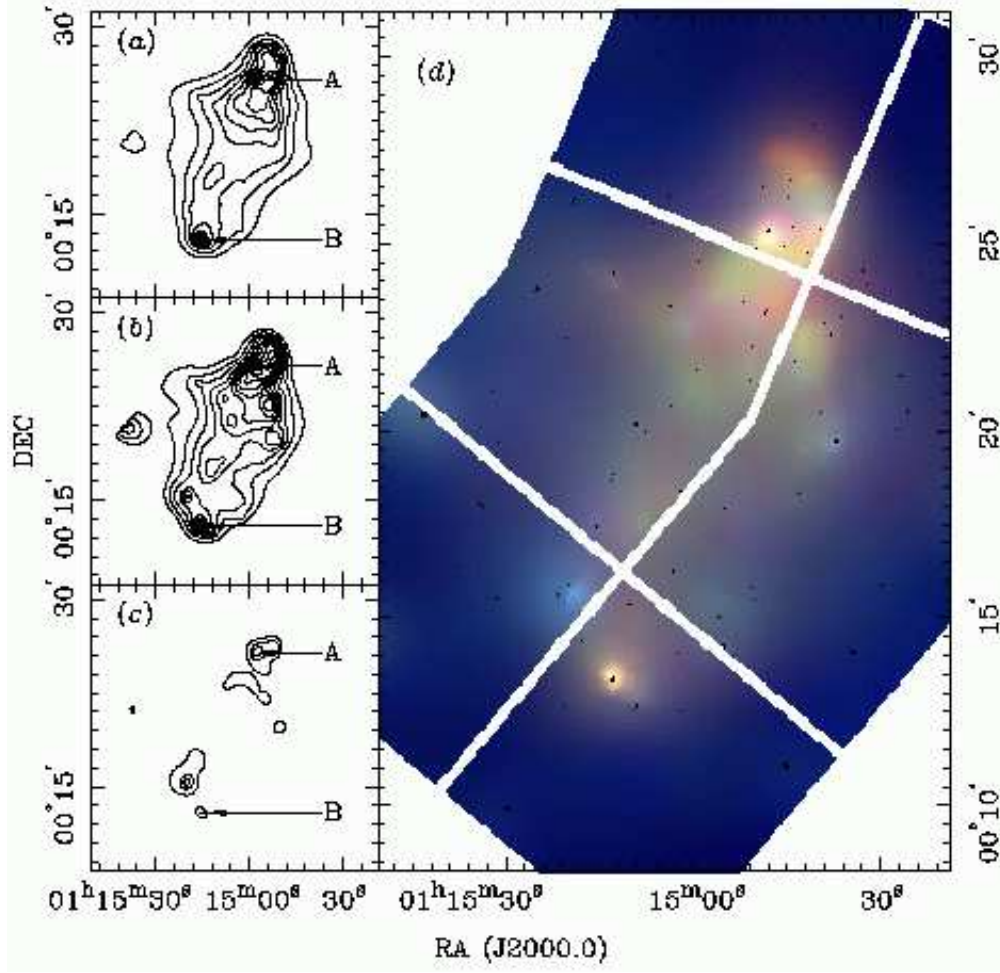


Fig. 3.— Panel *a*, *b*, *c* show the contours of soft (0.3-1.5 keV), medium (1.5-2.5 keV) and hard bands (2.5-10 keV), respectively. The signal-to-noise ratio for contours in both *a* and *b* are greater than  $5\sigma$ . Contours for panel *c* vary from  $3\sigma$  to  $8\sigma$ . The two X-ray peaks are labeled as A and B. Panel *d* shows a three-color image created by combining (linearly) the three band images. Redder regions represent the cooler regions; bluer regions indicate the hotter regions. Black points are removed point sources (see Figure 2 for clearer view of the point sources). [See the electronic edition of the Journal for a color version of this figure.]

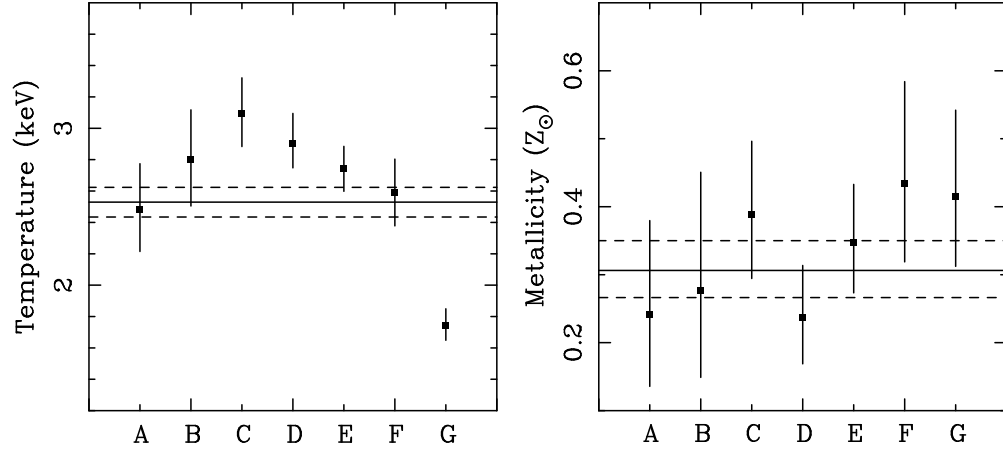


Fig. 4.— Temperature and metallicity for region A to G defined in Figure 1. In each panels, the solid and dashed lines indicate the mean value and the 90% error bars, respectively.



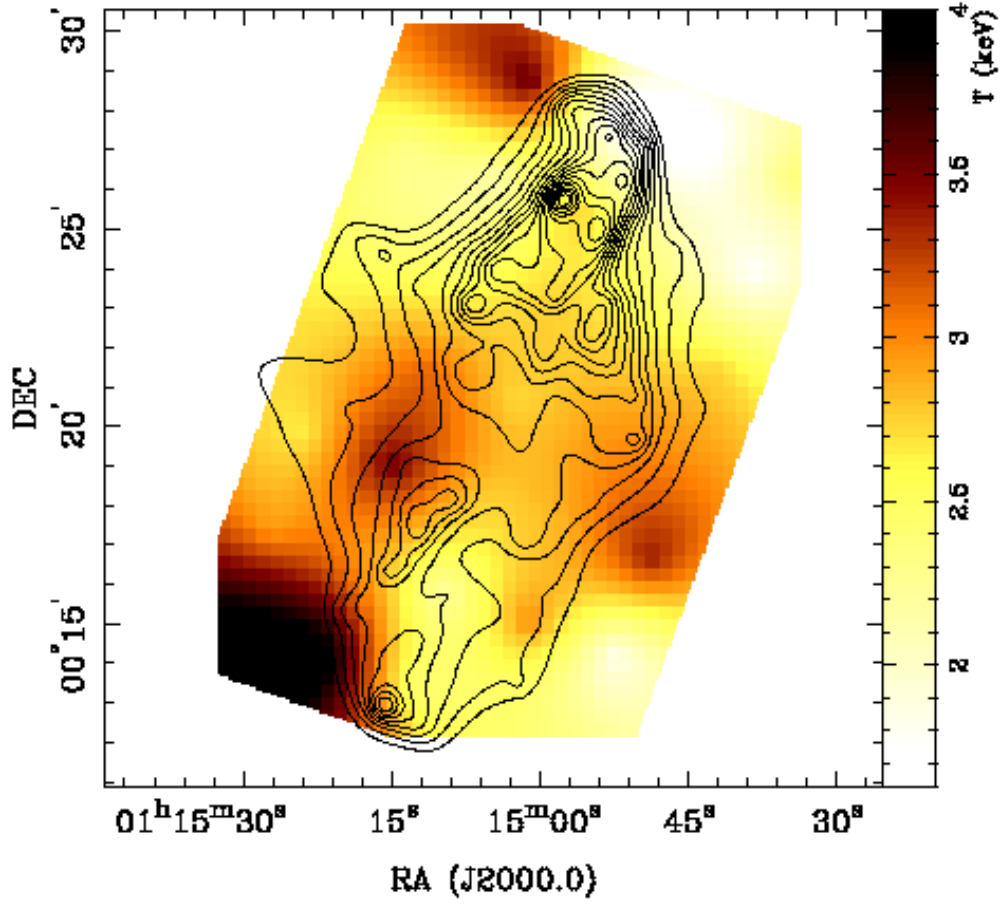


Fig. 5.— Contours ( $> 3\sigma$ ) of the adaptively smoothed image are overlaid on the temperature map. [See the electronic edition of the Journal for a color version of this figure.]

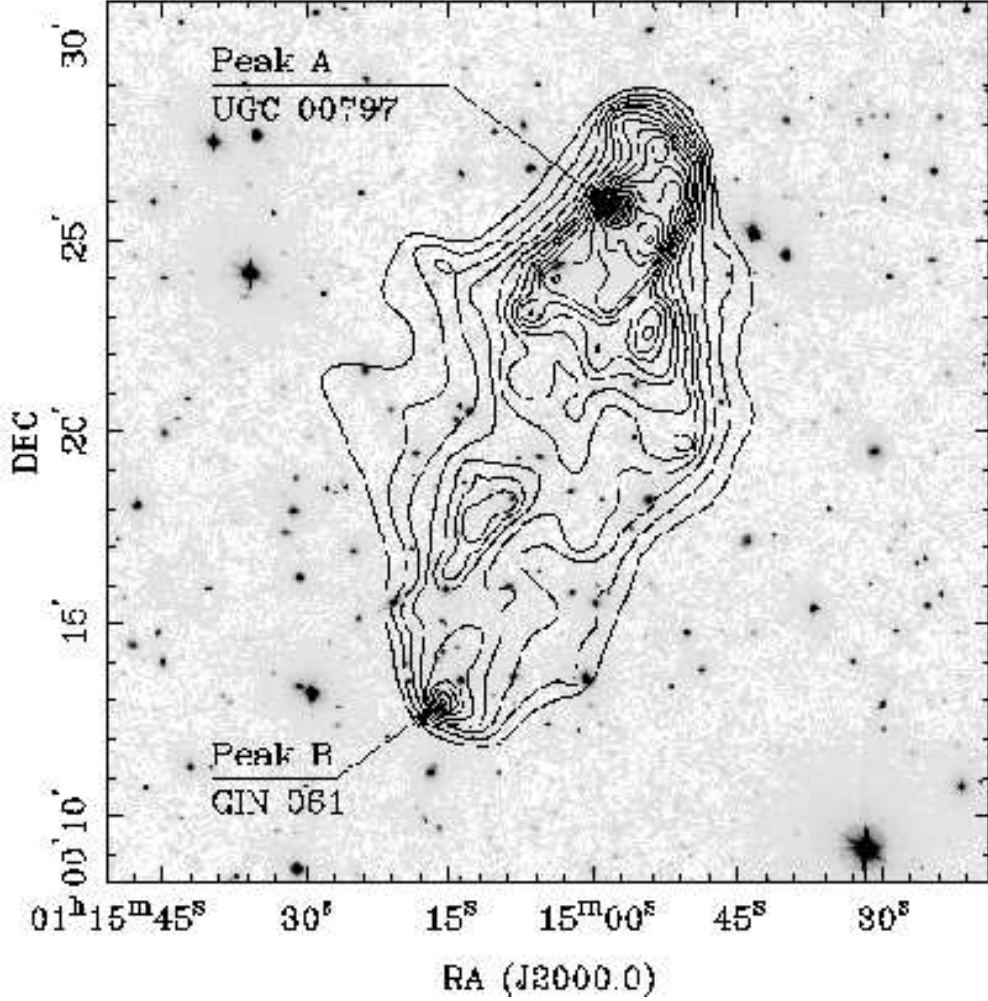


Fig. 6.— The X-ray contours ( $> 3\sigma$ ) is superposed on the optical BATC *i*-band image [BATC is a 15-color photometry program, see e.g., Fan et al. (1996) and Zhou et al. (2003)]; the values in the Chandra CCD gaps have been obtained by interpolation. The two X-ray peaks are labeled as A and B. Peak A is associated with the cD galaxy UGC 797. Peak B is very close to the second brightest member GIN 061, an elliptical galaxy. An elongated filament along the two peaks is clearly seen in the contours.

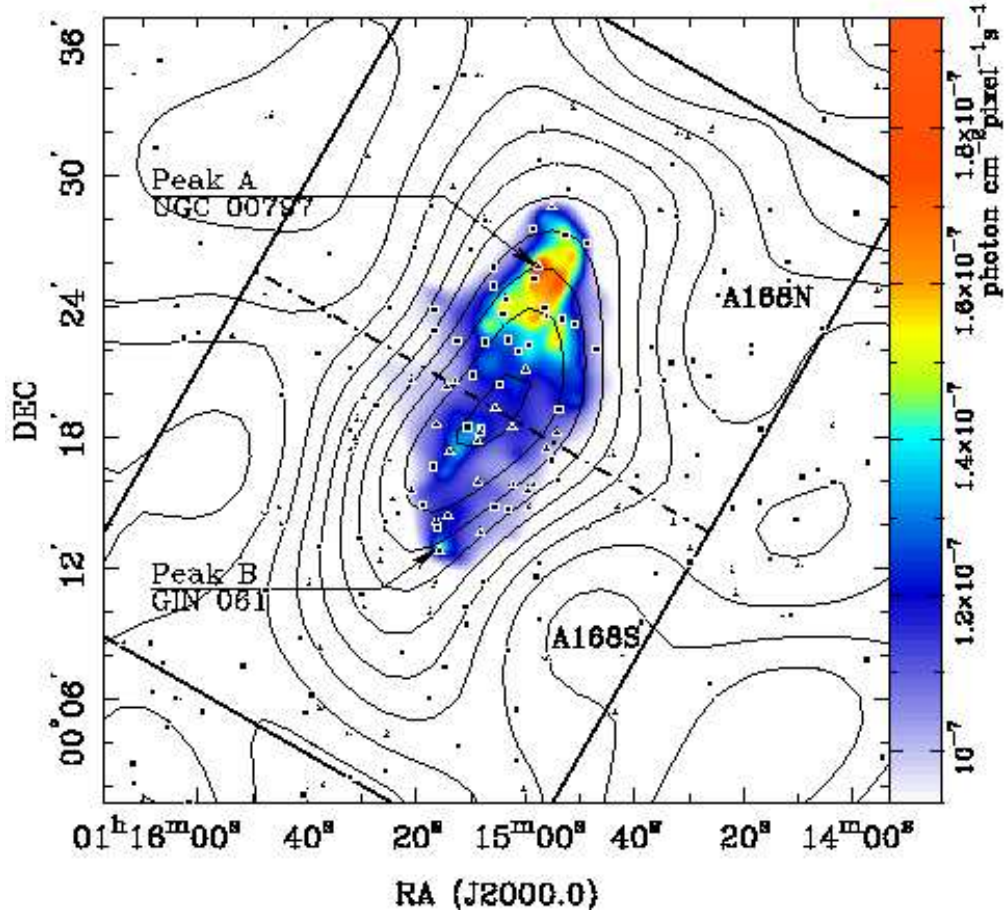


Fig. 7.— The *Chandra* X-ray image is overlaid on the contours of member galaxies distribution (cf. Paper I). The box (thick-line) separated by a dotted-dashed line indicates the two subclusters (A168N and A168S), as suggested in Paper I. The positions of member galaxy are also shown in the figure: filled-triangles are for the spectroscopically-selected members while the filled-squares indicate the members with photometric redshifts (cf. Paper I). [See the electronic edition of the Journal for a color version of this figure.]